



Investigations on the contact-electro-catalysis under various ultrasonic conditions and using different electrification particles[☆]

Xuanli Dong^{a,b}, Ziming Wang^{a,b}, Andy Berbille^{a,b,c}, Xin Zhao^a, Wei Tang^{a,b,*},
Zhong Lin Wang^{a,b,d,*}

^a CAS Center for Excellence in Nanoscience, Beijing Institute of Nanoenergy and Nanosystems, Chinese Academy of Sciences, Beijing 100083, China

^b School of Nanoscience and Technology, University of Chinese Academy of Sciences, Beijing 100049, China

^c CAS Center for Excellence in Nanoscience, National Center for Nanoscience and Technology (NCNST), Beijing 100190, China

^d School of Materials Science and Engineering, Georgia Institute of Technology, Atlanta, GA 30332-0245, USA

ARTICLE INFO

Keywords:

Contact electrification
Contact-electro-catalysis
Ultrasonic
Optimal conditions

ABSTRACT

Contact electrification (CE), as a well-known physical phenomenon, is widely used in energy, purifying applications. However, employing the electron-transfer in heterophase interfaces CE during mechanical stimulation to induce chemical reactions is rarely reported. Recently, the concept of contact-electro-catalysis (CEC) was proposed, which represents the reactivity of charge exchange at heterogeneous interfaces and the catalytic performance of pristine dielectric powders. In this study, we aim to investigate the optimal parameters for CEC under the ultrasonic reaction condition. We investigated the degradation of methyl orange (MO) solution by Fluorinated Ethylene Propylene (FEP) powder under different ultrasonic powers of 120 W, 240 W, 360 W, 480 W, 600 W, and different frequencies of 20 kHz, 28 kHz, 40 kHz and 89 kHz, in 240 min. The experimental results showed that the final degradation rate of MO increases with the increase of ultrasonic power. And the highest final degradation rate was obtained at the ultrasonic frequency of 40 kHz. Meanwhile, it is found that a highest reaction rate was achieved around 22 °C with the FEP as the catalyst in our experiment. Furthermore, we studied the effect of different dielectric particles on the organic solutions' decolorization. It is found that the CEC degradation is more prone to occur in the catalyst with strong electron-withdrawing ability (e.g. FEP vs. MO), while apparent physical adsorption occurs when the catalyst and the targeted organic ions possess opposite electric polarity (e.g. Nitrile Butadiene Rubber (NBR) vs. MO, or FEP vs. Rhodamine B (RhB)). This study helps to characterize the optimal conditions and the further understanding of CEC reactions and catalysts.

1. Introduction

Contact electrification (CE) has been discovered for more than 2600 years due to its universality. Since 2012, CE based triboelectric nanogenerator has been widely used in many fields, such as the harvesting of body motion energy [1,2], the collection of vibration [3,4], wind [5–7], rain [8,9] energy, large-scale water wave energy harvesting [10–12] self-powered internet of things [13,14], and wearable sensing [15,16]. Recently, the research on the contact electrification mechanism of the liquid-solid interface has been reported [17,18], which demonstrated

that the electrons play a dominant role in the charge transferring occurring at the interface. Therefrom, the mechanism of contact-electro-catalysis (CEC) has been proposed [19]. It is based on the contact electrification induced electron transfer among the dielectric material, reactant or surrounding medium. Considering the ubiquity of the materials electrification property, CEC broadens the selection of catalyst materials, compared to the traditional metal-based- [20], enzyme- [21], organo- [22] catalysis, as well as photocatalysis [23,24], piezocatalysis [25–27] and so on.

In this paper, taking the degradation of methyl orange (MO) as an

[☆] "Prof Zhong Lin Wang, an author on this paper, is the Editor-in-Chief of Nano Energy, but he had no involvement in the peer review process used to assess this work submitted to Nano Energy. This paper was assessed, and the corresponding peer review managed by Professor Chenguo Hu, also an Associate Editor in Nano Energy"

* Corresponding authors at: CAS Center for Excellence in Nanoscience, Beijing Institute of Nanoenergy and Nanosystems, Chinese Academy of Sciences, Beijing 100083, China.

E-mail addresses: tangwei@binn.cas.cn (W. Tang), zhong.wang@mse.gatech.edu (Z.L. Wang).

<https://doi.org/10.1016/j.nanoen.2022.107346>

Received 21 February 2022; Received in revised form 19 April 2022; Accepted 1 May 2022

Available online 11 May 2022

2211-2855/© 2022 Elsevier Ltd. All rights reserved.

example, we investigated the optimal parameters for CEC, including the ultrasonic power, frequency, temperature, as well as different catalysts. Experimental results show that the best CEC performance is obtained at 40 kHz and 600 W, and 20–30 °C is the optimal temperature range. As for catalytic materials, we found that the CEC degradation is more prone to occur in the catalyst with strong electron-withdrawing ability (e.g. Fluorinated Ethylene Propylene (FEP) vs. methyl orange (MO)), while apparent physical adsorption occurs when the catalyst and the targeted organic ions possess opposite electric polarity (e.g. Nitrile Butadiene Rubber (NBR) vs. MO, or FEP vs. Rhodamine B (RhB)).

2. Experimental

2.1. Sample preparation

Methyl orange [$C_{14}H_{13}N_3NaO_3S$, Macklin, 98%; Molecular weight: 327.33], rhodamine B [$C_{28}H_{31}ClN_2O_3$, Macklin, 99%; Molecular weight: 479.01], methylene blue [$C_{16}H_{18}ClN_3S$, Macklin, 98%; Molecular weight: 319.85], fluorinated ethylene propylene (FEP) [$(C_3F_6-C_2F_4)_n$, Dupont; Density: 2.15 g/cm³; Particle size: 3 μm], polyvinylidene fluoride (PVDF) [$(C_2H_2F_2)_n$, SOLVAY; Density: 1.76–1.80 g/cm³; Particle size: 4 μm; Molecular weight: 320000–670000], nitrile butadiene rubber (NBR) [$(C_4H_6)_m(C_3H_3N)_n$, Kumho; Particle size: 4 μm; Molecular weight: ~700000], polyvinyl chloride (PVC) [$(C_2H_3Cl)_n$, Kumho; Density: 1.38 g/cm³ (25 °C); Molecular weight: 50000–110000], polyoxymethylene (POM) [$(CH_2O)_n$, Dupont; Density: 1.39–1.43 g/cm³ (25 °C); Particle size: 4 μm; Molecular weight: 20000–110000].

A 5-ppm solution of methyl orange was prepared from 5 mg of methyl orange and 1 L of ultrapure water and subjected to one hour of magnetic stirring. Approximately 20 mg of FEP powder was added to 50 mL of as-prepared methyl orange solution and stirred magnetically at 1000 rpm for 48 h. Then, the methyl orange solution containing the FEP powder was then subjected to ultrasonication in a single tank ultrasonic cleaner (Yumeng, JTS-1024) for 240 min. Aliquots were sampled at 0, 15, 30, 60, 120, 180 and 240 min. The particles after reactions were separated from the solution by using a vacuum filter and placed in a drying oven at 40 °C overnight. Deionized water was used through all experimental procedures and the water temperature changes in the ultrasonic cleaning bath were controlled by a copper cooling system.

2.2. Sample characterization

The concentration of methyl orange in aqueous solution was analyzed by UV-Vis spectrophotometer (Cary 3500 and Shimadzu UV-3600) at the characteristic wavelength.

Differential scanning calorimetry (DSC) test was performed on a PerkinElmer differential scanning calorimeter DSC6000. The test atmosphere was nitrogen and the heating rate was 20 °C/min, the temperature range was 20–200 °C and maintained for 3 min. Then the temperature was cooled down to 0 °C at a rate of 50 °C/min and maintained for 3 min. This process eliminated the material thermal history and finally increased the temperature from 0 °C to 200 °C at a rate of 20 °C/min. The glass transition temperature of FEP was measured during this process.

The X-ray photoelectron spectroscopy analysis was performed on a Thermo Fisher Scientific Nexsa, USA. The chamber vacuum was 5×10^{-9} mBar, using an Alka ray source ($h\nu=1486.6$ eV). The operating voltage was 12 kV and the filament current was 6 mA. The test signal was accumulated for 5–50 cycles. The full-spectrum test pass-energy (Passing-Energy) was 200 eV in 1 eV steps and the narrow-spectrum test pass-energy (Passing-Energy) was 50 eV in 0.1 eV steps, with a charge correction using C1s= 284.80 eV binding energy as the energy standard.

The Liquid chromatography–mass spectrometry (LC-MS) analyses were conducted using a Thermo Scientific Q Exactive Orbitrap Quadrupole-Electrostatic Field Orbitrap High-Resolution Tandem Mass

Spectrometer. The HESI ion source of the mass spectrometer was set at – 3.0 kV, in positive ion mode. The mass spectrometry scanner was set on the full scan range of 100–1000 *m/z*. The column used was Hypersil Gold C18 (2.1 *100 mm, 1.9 μm) and the column temperature was 40 °C. The flow rate is 0.3 mL/min and the injection volume is 5 μL. Mobile phase A was composed of 0.1% formic acid aqueous solution, and mobile phase B was an acetonitrile solution. The temperature of the sample tray is 8 °C.

3. Results and discussion

3.1. The overall experimental setup

The main part of the experimental setup is shown in Fig. 1a, and the degradation of MO by contact-electro-catalysis (CEC) is carried out in the ultrasonic reaction bath. This ultrasonic chamber can be set to four frequencies of 20 kHz, 28 kHz, 40 kHz and 89 kHz and a maximum input power of 600 W. The acrylic plate serves as a beaker support and the bottom of the beaker is approximately 1 cm away from the ultrasound probe at the bottom of the reaction chamber. The initial temperature of all reactions was 20 °C. In order to modulate the water temperature during the sonication process, a copper pipe cooling system was introduced to the setup. The volume of deionized water in the reaction bath is fixed at 8.55 L in order to obtain a larger actual power input and more convenient to compare the power density under different powers. Fig. 1b shows the overall experimental process of the parameter's optimization of CEC reaction. According to the CEC principle [19], due to the propagation of ultrasonic waves in the solution, the formation, growth and collapse processes of cavitation bubbles are induced. This extremely intense process not only provides the conditions for the frequent contact-separation cycles between FEP and water, but also promotes the electron transfer between the two during contact electrification. After the interaction with water, the FEP surface becomes negatively charged. At the same time, the bursting of the cavitation bubbles causes the oxygen molecules contained therein to be released during the process and to grab electrons once they collide with the charged catalyst surface. This cycle is repeated as long as the ultrasonication sustains. As a result, oxygen that captured electrons forms superoxide radicals and gives rise to the formation of hydroxyl radicals by a chain reaction. These reactive radicals can react with the target organic molecules (e.g., methyl orange). In our experiments, 48 h of stirring prior to ultrasonication is performed for all experiments, to achieve better contact between FEP and water. Then, beakers containing suspension are placed in the ultrasonic reaction bath.

3.2. Ultrasonic parameter optimization

CEC is activated by the process of cavitation bubble formation, growth and collapse, while ultrasonic power and frequency determine the two main parameters of cavitation bubbles, i.e. number and size. In order to investigate the effect of ultrasonic parameters on the performance of CEC, we compared the degradation of methyl orange (MO) with FEP as the CEC catalyst, at different input powers (60 W, 120 W, 240 W, 360 W, 480 W and 600 W) under different ultrasonic frequencies of 20 kHz, 28 kHz, 40 kHz and 89 kHz in 240 min. The concentration curves of MO obtained by UV-Vis spectroscopy under the ultrasonic frequency of 40 kHz with different powers are plotted in Fig. 2a. The results under frequencies of 20 kHz, 28 kHz and 89 kHz are shown in the Supplementary Fig 1. As we can see, the degradation rate of MO gradually increased with the increase of power from 60 W to 600 W. As a comparison, Supplementary Fig. 2 shows that little degradation of MO occurs in the absence of ultrasonication, as well as in the absence of catalyst. Fig. 2b illustrates the final degradation rate of MO under various ultrasonic powers with the frequency of 40 kHz. The final removal efficiency increases with the power from 1.04% of 60 W to 98.31% of 600 W. The experimental results show that a larger power

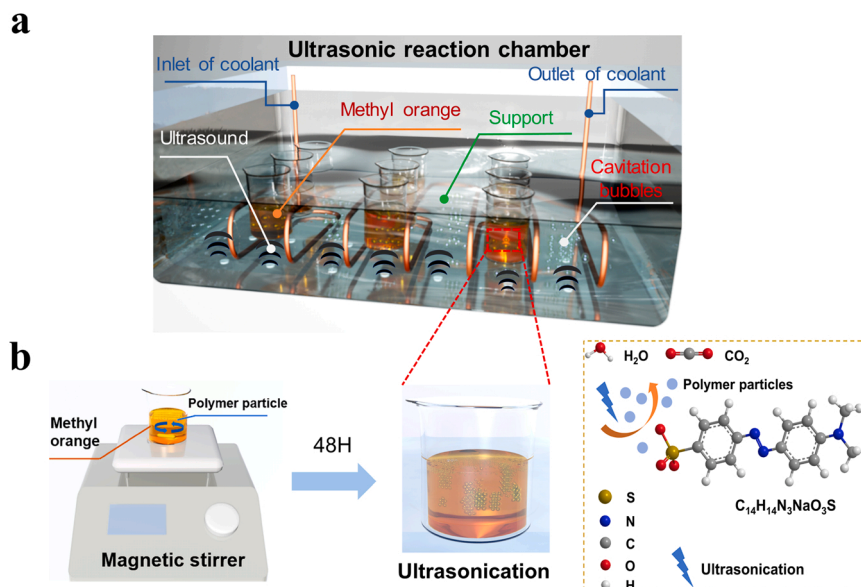


Fig. 1. The overall experimental setup and experimental protocol. (a) Ultrasonic reaction bath; (b) The experimental protocol and CEC degradation diagram.

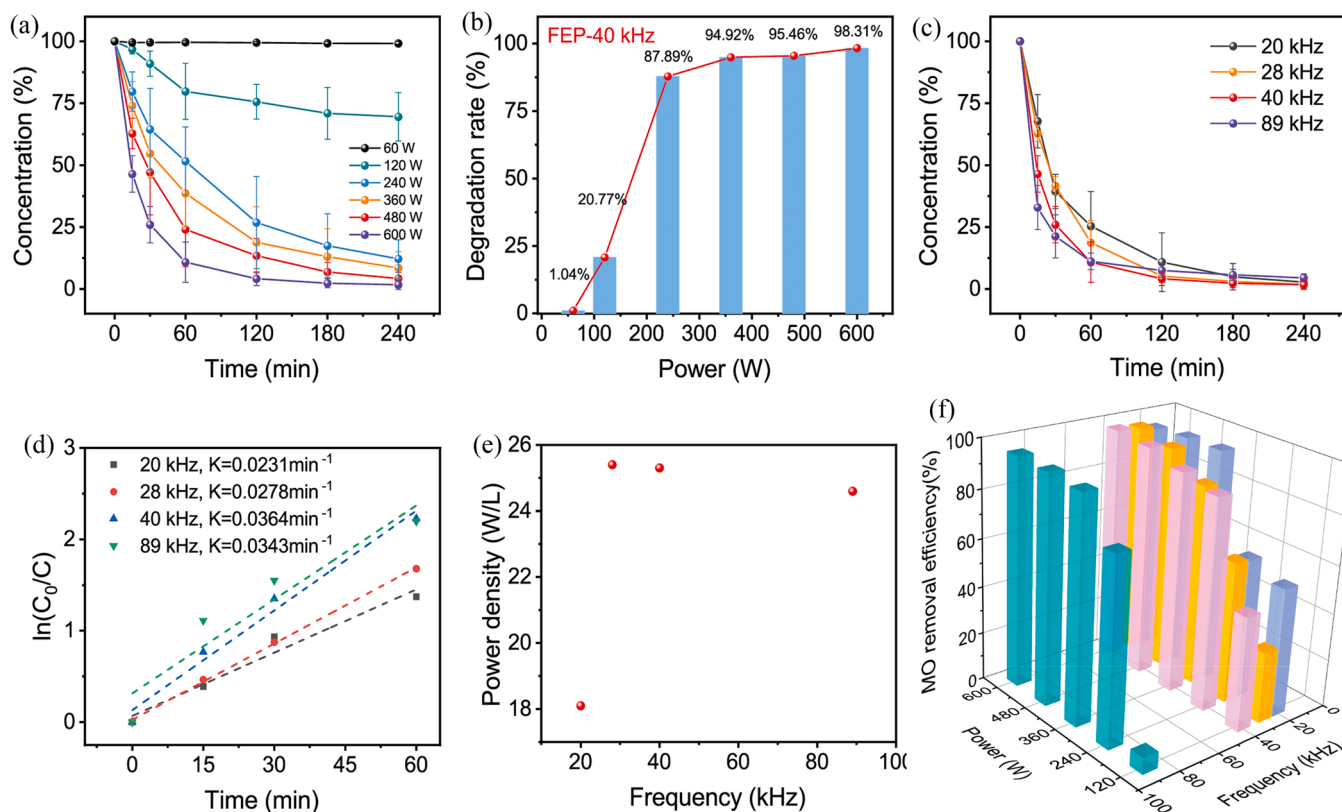


Fig. 2. Effect of different ultrasonic parameters on the degradation of methyl orange (MO). (a) Effect of different power (60 W, 120 W, 240 W, 360 W, 480 W and 600 W) on the degradation of MO by FEP at 40 kHz. (b) The maximum MO removal efficiency evolution corresponding to each power at 40 kHz. (c) Evolution of UV-Vis absorbance of MO at four frequencies (20 kHz, 28 kHz, 40 kHz and 89 kHz). (d) Kinetic constants of MO degradation at the frequency of 20 kHz, 28 kHz, 40 kHz and 89 kHz. (e) Evolution of ultrasonic power density at different frequencies. (f) Final removal efficiency of MO at different frequencies and powers.

input will promote the degradation of MO by CEC because large ultrasonic power induces a higher number of cavitation bubbles and energy. Fig. 2c compares the degradation at different ultrasonic frequencies with the power of 600 W, and Fig. 2d shows the kinetic constants [28] (Supplementary Note 1) corresponding to four frequencies. Owing to the degradation of MO molecule itself mainly happens at the first stage, only

the change of MO concentration in the first 60 min was studied according to the previous study [19]. The reaction kinetic constants of MO at 600 W increases with frequencies (20 kHz, 28 kHz, 40 kHz, 89 kHz) as follows: 0.0231 min^{-1} , 0.0278 min^{-1} , 0.0364 min^{-1} and 0.0343 min^{-1} . In addition, the corresponding maximum removal efficiency of MO at the four frequencies are 97.30%, 98.14%, 98.31% and

95.51%, respectively (Supplementary Fig. 3). Therefore, we can conclude that 40 kHz and 600 W are the best ultrasonic parameters for CEC reaction in our experiments, with a highest decolorization rate (98.31%) of MO and a highest reaction rate constant (0.0364 min^{-1}). The CEC degradation performance is largely determined by the contact separation cycles between water and catalyst (frequency) and the actual energy dispersed in the reaction system (power), and in our experiments, the latter varies with the former. Therefore, we measured the ultrasonic power density as a bulk effect to explain the differences in CEC degradation at different frequencies using calorimetry method [29] (Fig. 2e). We measured the temperature (T) rise versus time (t) using an electronic digital thermometer with an interval of 15 min and a sampling frequency of four times (Supplementary Fig. 4). From the T versus t data, a linear fit was made to the data to obtain the rate of change of temperature, dT/dt . All measurements of temperature are repeated three times to ensure more accurate results. In this study, the liquid phase medium is deionized water and the volume is fixed at 8.5 L. Fig. 2e shows that the ultrasonic power density (Supplementary Note 2) increases with the ultrasonic frequency as 18.1 W/L, 25.4 W/L, 25.3 W/L and 24.6 W/L. The highest power density was obtained in the range of 28–40 kHz, which is consistent with the above MO's degradation experimental results. Fig. 2f shows the removal rate of MO for all ultrasonic parameters, and the experimental results illustrate that the final degradation rate is closely related to the power density.

3.3. The effect of temperature on CEC performance

In order to obtain the effect of temperature change on the performance of CEC, we compared the final degradation rate of methyl orange by FEP at 10 °C, 20 °C, 30 °C, 40 °C and 50 °C, respectively. The experimental results are shown in Fig. 3a, which indicates the degradations at 20 °C, 30 °C are obviously faster. The reaction rate constants are calculated and plotted in the Fig. 3b. It tends to increase and then decrease with the increasing temperature and reaches a maximum degradation rate of 0.0364 min^{-1} at around 22 °C. In addition, the final removal rate can be found in Supplementary Fig. 5, and it increased from 66.5% at 50 °C to 97.7% at 20 °C within 180 min. From this study, it appears that the most favorable temperature for the CEC process lies between 20 °C and 30 °C. We speculate that the FEP powder undergoes a glass transition process [30] in our experiments when the temperature beyond a certain value. And the differential scanning calorimetry (DSC) results presented in Fig. 3c verify this assumption. The glass transition temperature is around 35 °C, that is, the changing viscosity and softening of the polymer particles above the glass transition region affect the CEC process. Nevertheless, the temperature influence might be complex, further experiments are required for a deep understanding.

3.4. Investigations on different catalysts (dielectric materials) of CEC

In addition to the environmental conditions, the contact electrification performance of the catalytic material itself also dominates the performance of the CEC reaction. We selected different dielectric materials, including electronegative materials (Polyvinyl chloride (PVC), Polyvinylidene difluoride (PVDF), FEP), and electropositive materials (Nitrile Butadiene Rubber (NBR), Ethyl cellulose (EC), Polyoxymethylene (POM)), to investigate the decolorization rate of MO. In the case of single particles (Fig. 4a, and b), the total amount of catalyst was 20 mg. And in the case of particle combinations (Fig. 4d-i), the total amount of each catalyst was 10 mg. Fig. 4a, and b show the decolorization of MO by three electronegative particles and three electropositive particles, respectively. The reaction in the presence of FEP showed a higher decolorization rate of MO overall. According to the literature [17], the electron-withdrawing (EW) ability of a polymer is related to the elemental type of its side chain functional groups and the degree of unsaturation of the functional groups. The presence of F atoms in the side chains lead to a higher charge density [17] in contact with water due to the strong EW ability of the F group, while the content of the F element also directly determines the electronegativity of the polymer. Therefore, the amount of transferred charge decreases sequentially with FEP (polyfluoro), PVDF (bifluoro), and PVC (without F) during the electrification process. Hence, the FEP shows a better degradation performance. In addition, we studied the degradation of methyl orange by FEP powders of different particle sizes as shown in Supplementary Fig. 6. The final degradation rate of methyl orange underwent a considerable change, increasing from 28.9% to 98.31% with the decrease of FEP particle size. And the FEP particles of 3 μm showed the highest kinetic reaction constants ($K=0.0364 \text{ min}^{-1}$). These results imply that there may be a critical size of the catalyst particle size to activate an effective CEC process. Whereas, the reaction activated by electropositive particles were obviously low. We examined the C1s and O1s X-ray photoelectron spectroscopy (XPS) energy spectra of NBR Rubber particles before and after the reaction, as shown in Supplementary Fig. 7a, b, respectively. No shift in the binding energy of the original peaks was observed after the reaction by using NBR particles, which demonstrates the stability of electropositive particles in the CEC process. However, new peaks of S appear on the NBR particles spectrum (Fig. 4c), which could come from the MO molecule, indicating the MO molecule's physical absorption. This is apparently different from the experimental results that by electronegative particles. Subsequently, we studied the decolorization of MO by the mixed particles with PVC, PVDF and FEP as electronegative materials, and NBR Rubber, EC and POM as electropositive materials (Fig. 4d-i). The experimental results show that the EW ability of the electronegative particles in the CEC process dominates the extent to which the reaction proceeds. In the mixed reaction

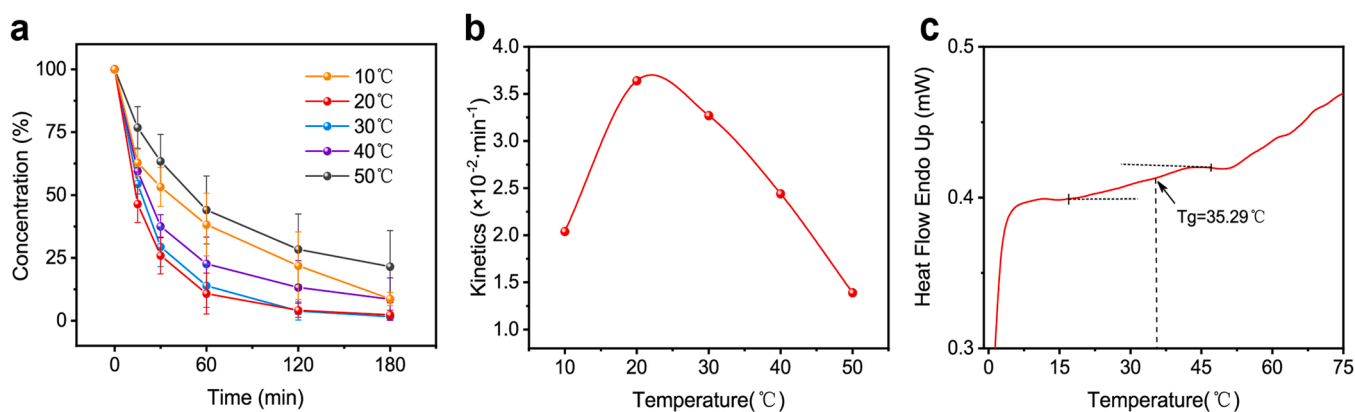


Fig. 3. Effect of different temperatures on CEC performance. (a) Evolution of UV-Vis absorbance of methyl orange at 10 °C, 20 °C, 30 °C, 40 °C and 50 °C, respectively. (b) Degradation kinetics. (c) Differential scanning calorimetry result for FEP powders and T_g indicates the glass transition temperature.

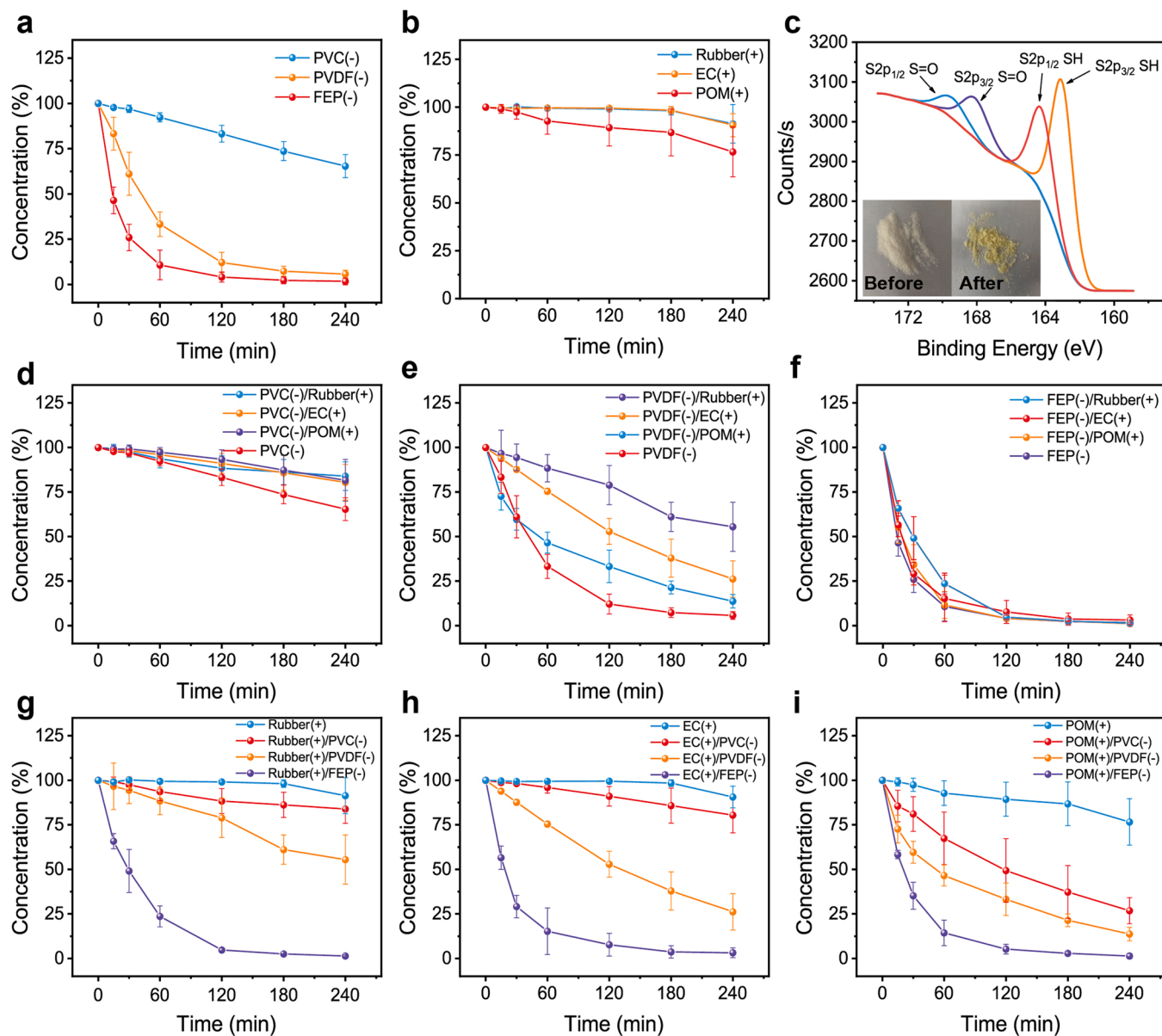


Fig. 4. Evolution of UV-Vis absorbance of the methyl orange solution during ultrasonication with different particle combinations. (a) Evolution of UV-Vis absorbance of the methyl orange solution in the presence of different electronegative particles (PVC, PVDF, FEP). (b) Evolution of UV-Vis absorbance of the methyl orange solution in the presence of different electropositive particles (NBR Rubber, EC, POM). (c) S2p X-ray photoelectron spectroscopy (XPS) spectrum of NBR after the reaction. Inset of c: Optical photos of NBR powder before and after the CEC process. Decolorization of MO in the presence of (d) PVC, (e) PVDF and (f) FEP (electronegative particles) in the particle combination system, respectively. Decolorization of MO in the presence of (g) NBR Rubber, (h) EC and (i) POM (electropositive particles) in the particle combination system, respectively.

system, the final decolorization rate of MO increased with the EW ability of the electronegative particles, from a lowest of 16.2% for the PVC/NBR to a highest of 98.6% for the FEP/NBR. Specifically, the final decolorization of MO reached 98.6%, 96.8% and 98.6% in the presence of FEP in combination with NBR, EC and POM particles, respectively.

Considering the MO is a salt ($C_{14}H_{14}N_3SO_3Na$), the targeted organic ions ($C_{14}H_{14}N_3SO_3$) should be negative, and the FEP shows an excellent CEC ability in the above experiments. Therefore, rhodamine B ($C_{28}H_{31}ClN_2O_3$, RhB) and methylene blue ($C_{16}H_{18}ClN_3S$, MB), with their targeted organic ions positive, are selected to reperform the reaction. Specifically, FEP vs. MO, FEP vs. RhB, FEP vs. MB, POM vs. MO, POM vs. RhB and POM vs. MB are checked. And results are plotted in Fig. 5a.

It indicates that the set of FEP vs. RhB shows the fastest decreasing rate, followed by the set of FEP vs. MO. While the set of POM vs. RhB shows the lowest decreasing rate, and that of POM vs. MO is a bit higher.

Furthermore, liquid chromatography-mass spectrometry (LC-MS) analyses were performed to investigate the chemical degradation during the CEC process. From Fig. 5b-c, we can see that there is scarcely any chemical degradation in the set of POM vs. RhB, while in the case of POM vs. MO, obvious chemical degradation was obtained. And considering that the decrease in the intensity of the main peak is contributed by both physical adsorption and chemical degradation, we can calculate the area of each ion peak (see Supplementary Fig. 8), and presume that the proportion of chemical degradation, physical adsorption, and undecomposed MO during 240 min of ultrasonication were: 26.8%, 49.6%, and 23.6%, respectively. The normalized ratios of chemical degradation and physical adsorption were: 35.1%, 64.9%, respectively. On the other side, Fig. 5d shows that FEP successfully degraded the MO molecules (based on the data from the previous study [19] of the degradation of MO by FEP powder), but in the case of FEP vs. RhB (Fig. 5e), no apparent

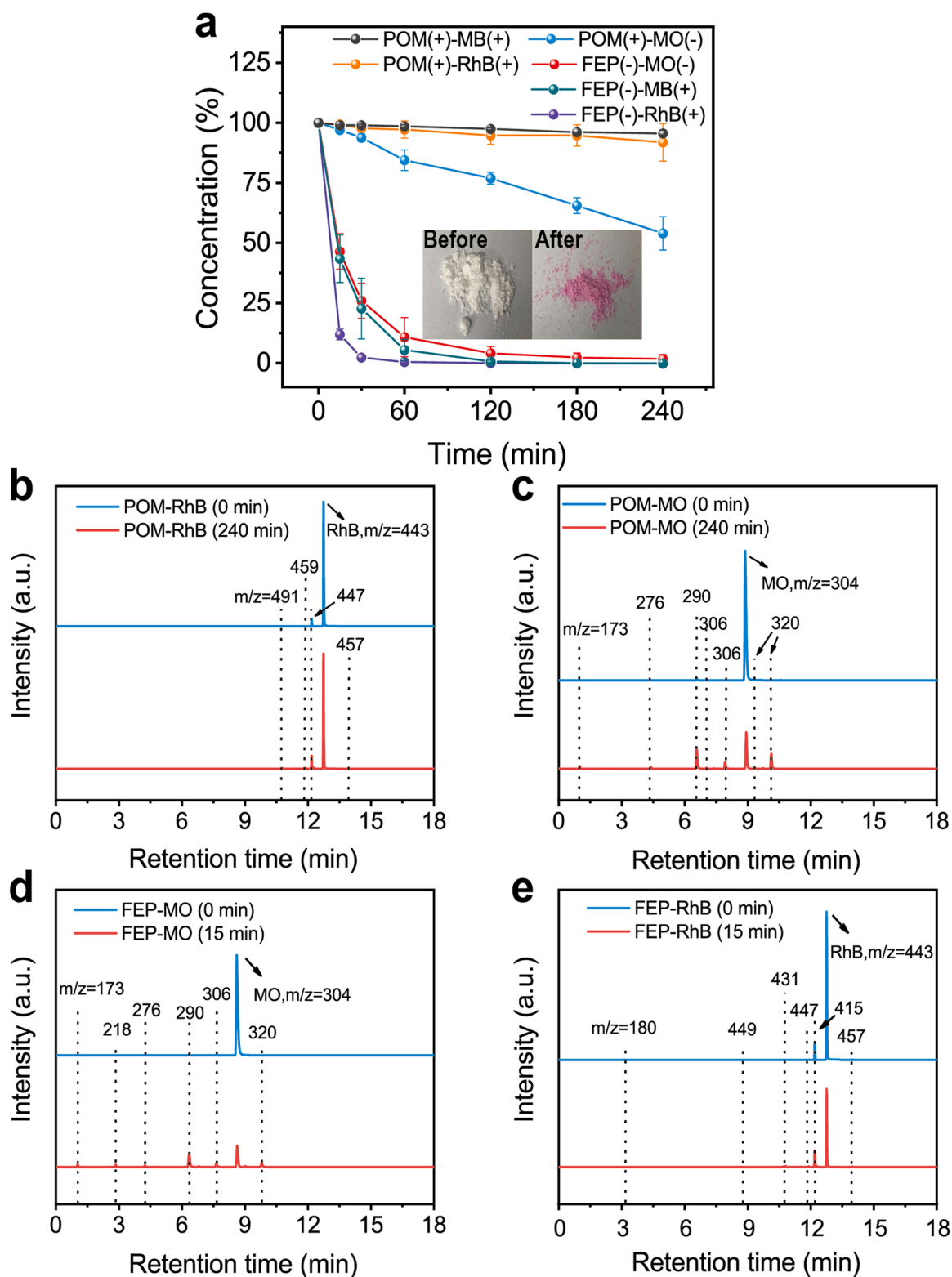


Fig. 5. Decolorization of organic molecules with different electric polarities in the presence of different catalyst materials. (a) UV-vis spectra of RhB solution (positive polarity) and MO solution (negative polarity) in the presence of different catalysts (FEP, negative; POM, positive). Inset of a: Optical photos of FEP powder before and after CEC process (Before: 0 min; After: 240 min). (b) Liquid chromatography-mass spectrometry (LC-MS) analysis of RhB solution in the presence of POM (0 min, 240 min). (c) LC-MS analysis of MO solution in the presence of POM (0 min, 240 min). (d) LC-MS analysis of MO solution in the presence of FEP (0 min, 15 min). (e) LC-MS analysis of RhB solution in the presence of FEP (0 min, 15 min).

degradation was found around 15 min. However, the latter's UV-Vis test shows the fastest decreasing rate, which suggests that when CEC catalyst's polarity is opposite to that of the targeted degradation ions, physical adsorption will take the priority, leading to the catalytic performance inhibition. The LC-MS analyses of the decolorization of MB solution by POM and FEP are shown in [Supplementary Fig. 9](#). Both positively charged dyes showed similar decolorization behaviors in the presence of FEP and POM as the catalysts.

At last, we varied the total amount of particles to study the decolorization of MO with different particle combination systems and single particle systems, respectively ([Supplementary Fig. 10](#)). It is found that there may be a saturation value for the amount of dielectric particles introduced for degradation. For instance, in our experiment, the saturation amount of FEP is about 10 mg, for degrading 5 mg/L MO solution with a volume of 50 mL.

4. Conclusions

In conclusion, the performance of degradation of MO by CEC under different ultrasonic parameters (Frequencies of 20 kHz, 28 kHz, 40 kHz, 89 kHz and powers of 120 W, 240 W, 360 W, 480 W, 600 W) and different temperatures (10 °C, 20 °C, 30 °C, 40 °C and 50 °C) was studied. The effect of different ultrasonic parameters on CEC was investigated by FEP powder on the degradation of MO solution at 20 °C. Experimental results show that 40 kHz and 600 W are the best ultrasonic condition for CEC in our experiments, and 20–30 °C is the optimal temperature range for the case of FEP. By investigating the effect of different catalysts for CEC reaction, we found that the performance of CEC degradation is determined by the electronegative materials. And the chemical degradation is more prone to occur in the catalyst with the strong electron-withdrawing ability (e.g. FEP vs MO), while apparent physical adsorption occurs when the catalyst and the targeted organic ions possess opposite electric polarity (e.g. NBR vs MO, or FEP vs RhB) and physical adsorption affects the final degradation rate of organic molecules during the CEC process. Our research provides detailed instructions for the performing of CEC process under ultrasonic condition, as well as a further understanding of CEC and CEC catalysts.

CRedit authorship contribution statement

Xuanli Dong: Investigation, Formal analysis, Visualization, Writing – original draft. **Ziming Wang:** Investigation, Writing – review & editing. **Andy Berbille:** Investigation, Writing – review & editing. **Xin Zhao:** Investigation. **Wei Tang, Zhong Lin Wang:** Conceptualization ideas, Writing – review & editing, Supervision, Project administration.

Declaration of Competing Interest

The authors declare that they have no known competing financial interests or personal relationships that could have appeared to influence the work reported in this paper.

Acknowledgements

This work was supported by the National Key R & D Project from Minister of Science and Technology (2021YFA1201601), National Natural Science Foundation of China (Grant No. 52192610).

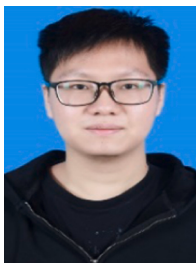
We would like to thank Yu Hou, Qinghang Zeng, Zhen Tang and Pengfei Chen for their assistance in the development of experimental setups and helpful discussions.

Appendix A. Supporting information

Supplementary data associated with this article can be found in the online version at [doi:10.1016/j.nanoen.2022.107346](https://doi.org/10.1016/j.nanoen.2022.107346).

References

- [1] P. Bai, G. Zhu, Z.-H. Lin, Q. Jing, J. Chen, G. Zhang, J. Ma, Z.L. Wang, Integrated multilayered triboelectric nanogenerator for harvesting biomechanical energy from human motions, *ACS Nano* 7 (2013) 3713–3719.
- [2] T.-C. Hou, Y. Yang, H. Zhang, J. Chen, L.-J. Chen, Z. Lin Wang, Triboelectric nanogenerator built inside shoe insole for harvesting walking energy, *Nano Energy* 2 (2013) 856–862.
- [3] Y. Qin, X. Wang, Z.L. Wang, Microfibre-nanowire hybrid structure for energy scavenging, *Nature* 451 (2008) 809–813.
- [4] X. Wang, T. Song, J. Liu, Z.L. Wang, Direct-Current Nanogenerator Driven by Ultrasonic Waves, *Science* 316 (2007) 102–105.
- [5] B. Chen, Y. Yang, Z.L. Wang, Scavenging wind energy by triboelectric nanogenerators, *Adv. Energy Mater.* 8 (2018), 1702649.
- [6] Y. Bian, T. Jiang, T. Xiao, W. Gong, X. Cao, Z. Wang, Z.L. Wang, Triboelectric nanogenerator tree for harvesting wind energy and illuminating in subway tunnel, *Adv. Mater. Technol.* 3 (2018), 1700317.
- [7] J. Park, M. Han, G. Kim, Y. Jung, H. Cho, Tree-wrapped triboelectric generator for harvesting wind energy, *J. Nanosci. Nanotechnol.* 20 (2020) 239–244.
- [8] Y.C. Lai, Y.C. Hsiao, H.M. Wu, Z.L. Wang, Waterproof fabric-based multifunctional triboelectric nanogenerator for universally harvesting energy from raindrops, wind, and human motions and as self-powered sensors, *Adv. Sci.* 6 (2019), 1801883.
- [9] X. Liu, A. Yu, A. Qin, J. Zhai, Soft electronics: hybrid 3D printing all-in-one heterogenous rigidity assemblies for soft electronics, *Adv. Mater. Technol.* 4 (2019), 1900680.
- [10] J. Chen, J. Yang, Z. Li, X. Fan, Y. Zi, Q. Jing, H. Guo, Z. Wen, K.C. Pradel, S. Niu, Z. L. Wang, Networks of triboelectric nanogenerators for harvesting water wave energy: a potential approach toward blue energy, *ACS Nano* 9 (2015) 3324–3331.
- [11] X. Liang, T. Jiang, G. Liu, T. Xiao, L. Xu, W. Li, F. Xi, C. Zhang, Z.L. Wang, Triboelectric nanogenerator networks integrated with power management module for water wave energy harvesting, *Adv. Funct. Mater.* 29 (2019), 1807241.
- [12] Z.H. Lin, G. Cheng, L. Lin, S. Lee, Z.L. Wang, Water-solid surface contact electrification and its use for harvesting liquid-wave energy, *Angew. Chem. Int. Ed. Engl.* 52 (2013) 12545–12549.
- [13] X. Cao, Y. Xiong, J. Sun, X. Zhu, Q. Sun, Z.L. Wang, Piezoelectric Nanogenerators Derived Self-Powered Sensors for Multifunctional Applications and Artificial Intelligence, *Adv. Funct. Mater.* 31 (2021), 2102983.
- [14] Y. Shao, M. Shen, Y. Zhou, X. Cui, L. Li, Y. Zhang, Nanogenerator-based self-powered sensors for data collection, *Beilstein J. Nanotechnol.* 12 (2021) 680–693.
- [15] Q. Jing, G. Zhu, W. Wu, P. Bai, Y. Xie, R.P.S. Han, Z.L. Wang, Self-powered triboelectric velocity sensor for dual-mode sensing of rectified linear and rotary motions, *Nano Energy* 10 (2014) 305–312.
- [16] L. Lin, S. Wang, S. Niu, C. Liu, Y. Xie, Z.L. Wang, Noncontact free-rotating disk triboelectric nanogenerator as a sustainable energy harvester and self-powered mechanical sensor, *ACS Appl. Mater. Interfaces* 6 (2014) 3031–3038.
- [17] S. Li, J. Nie, Y. Shi, X. Tao, F. Wang, J. Tian, S. Lin, X. Chen, Z.L. Wang, Contributions of different functional groups to contact electrification of polymers, *Adv. Mater.* 32 (2020), e2001307.
- [18] M. Sun, Q. Lu, Z.L. Wang, B. Huang, Understanding contact electrification at liquid-solid interfaces from surface electronic structure, *Nat. Commun.* 12 (2021) 1752.
- [19] Z. Wang, A. Berbille, Y. Feng, S. Li, L. Zhu, W. Tang, Z.L. Wang, Contact-electrocatalysis for the degradation of organic pollutants using pristine dielectric powders, *Nat. Commun.* 13 (2022) 1–9.
- [20] Z. Shao, H. Zhang, Combining transition metal catalysis and organocatalysis: a broad new concept for catalysis, *Chem. Soc. Rev.* 38 (2009) 2745–2755.
- [21] J.R. Knowles, Enzyme catalysis: not different, just better, *Nature* 350 (1991) 121–124.
- [22] E.N. Jacobsen, D.W.C. MacMillan, Organocatalysis, *Proc. Natl. Acad. Sci. U.S.A.* 107 (2010) 20618–20619.
- [23] M. Sharma, G. Singh, R. Vaish, Dye degradation and bacterial disinfection using multicatalytic BaZr_{0.02}Ti_{0.98}O₃ceramics, *J. Am. Ceram. Soc.* 103 (2020) 4774–4784.
- [24] H. You, Z. Wu, Y. Jia, X. Xu, Y. Xia, Z. Han, Y. Wang, High-efficiency and mechano-/photo- bi-catalysis of piezoelectric-ZnO@ photoelectric-TiO₂ core-shell nanofibers for dye decomposition, *Chemosphere* 183 (2017) 528–535.
- [25] Y. Feng, L. Ling, Y. Wang, Z. Xu, F. Cao, H. Li, Z. Bian, Engineering spherical lead zirconate titanate to explore the essence of piezo-catalysis, *Nano Energy* 40 (2017) 481–486.
- [26] X. Liu, L. Shen, W. Xu, W. Kang, D. Yang, J. Li, S. Ge, H. Liu, Low frequency hydromechanics-driven generation of superoxide radicals via optimized piezotronic effect for water disinfection, *Nano Energy* 88 (2021), 106290.
- [27] M. Pan, S. Liu, B. Pan, J.W. Chew, Directionally tailoring the macroscopic polarization of piezocatalysis for hollow zinc sulfide on dual-doped graphene, *Nano Energy* 88 (2021), 106312.
- [28] P.-J. Lu, C.-W. Chien, T.-S. Chen, J.-M. Chern, Azo dye degradation kinetics in TiO₂ film-coated photoreactor, *Chem. Eng. J.* 163 (2010) 28–34.
- [29] T.J. Mason, J.P. Lorimer, D.M. Bates, Quantifying sonochemistry: casting some light on a 'black art', *Ultrasonics* 30 (1992) 40–42.
- [30] S.S. Bair, High Pressure Rheology for Quantitative Elastohydrodynamics, Elsevier, 2019.



Xuanli Dong received his bachelor's degree from Beijing Information Science & Technology University in 2020. He is currently pursuing his master's degree in Beijing Institute of Nanoenergy and Nanosystems, Chinese Academy of Sciences. His research focuses on contact electrification at the liquid-solid interface and contact-electro-catalysis.



Wei Tang is a professor in Beijing Institute of Nanoenergy and Nanosystems, Chinese Academy of Sciences, Beijing, China. He received his B.S. and Ph.D. degrees from Peking University in 2008 and 2013. In recent years, he has been working on nanogenerators and wearable electronics. After graduation, he worked in Beijing Institute of Nanoenergy and Nanosystems as a postdoctoral research fellow. His research interests include wearable sensing, contact-electro-catalysis, contact electrification mechanisms at multiphase interfaces, and micro/nano processing.



Ziming Wang received his B.S. degree in Materials Science and Engineering from Central South University in 2017. Now he is a Ph.D. candidate in Beijing Institute of Nano Energy and Systems, Chinese Academy of Sciences. His research interests focus on self-powered sensors, energy harvesting, and contact-electro-catalysis.



Zhong Lin Wang received his Ph.D. degree from Arizona State University in physics. He now is the Hightower Chair in Materials Science and Engineering, Regents' Professor at Georgia Tech, the chief scientist and director of the Beijing Institute of Nanoenergy and Nanosystems, Chinese Academy of Sciences. Prof. Wang has made original and innovative contributions to the synthesis, discovery, characterization and understanding of fundamental physical properties of oxide nanobelts and nanowires, as well as applications of nanowires in energy sciences, electronics, optoelectronics and biological science. His discovery and breakthroughs in developing nanogenerators establish the principle and technological road map for harvesting mechanical energy from environmental and biological systems for powering personal electronics. His research on self-powered nanosystems has inspired the worldwide efforts in academia and industry for studying energy for micro-nano-systems, which is now a distinct disciplinary in energy research and future sensor networks. He coined and pioneered the fields of piezotronics and piezophototronics by introducing piezoelectric potential gated charge transport process in fabricating new electronic and optoelectronic devices.



Andy Berbille is a Ph.D. candidate in Zhong Lin Wang's group at the Beijing Institute of Nanoenergy and Nanosystems. After graduating from a joint master's program, in Materials Science and engineering, from UPEC, UPEM and ENPC in Paris, France, he was granted a CAS-TWAS President's Fellowship to pursue a PhD degree in the Chinese Academy of Sciences. His research interests cover energy materials, hydrogen storage, heterogeneous catalysis, soft materials, piezoelectric materials, magnetoelectric catalysis and contact-electrification.



Xin Zhao is currently an engineer work in Beijing Institute of Nanoenergy and Nanosystems, CAS. His current research focuses on contact-electro-catalysis.